Preprints.org

Article

Not peer-reviewed version

High-Resolution DLP 3D Printing for Complex Curved and Thin-Walled Structures at Practical Scale: Archimedes Microscrew

Chih-Lang Lin , Jun-Ting Liu , Chow-Shing Shin *

Posted Date: 24 June 2025

doi: 10.20944/preprints202506.1976.v1

Keywords: projection micro-stereolithography (PμSL); DLP 3D printing; microfluidic component; archimedes microscrew; photo-polymerization

Preprints.org is a free multidisciplinary platform providing preprint service that is dedicated to making early versions of research outputs permanently available and citable. Preprints posted at Preprints.org appear in Web of Science, Crossref, Google Scholar, Scilit, Europe PMC.

Copyright: This open access article is published under a Creative Commons CC BY 4.0 license, which permit the free download, distribution, and reuse, provided that the author and preprint are cited in any reuse.

Preprints.org (www.preprints.org) | NOT PEER-REVIEWED | Posted: 24 June 2025 doi:10.20944/preprints202506.1976.v1

Disclaimer/Publisher's Note: The statements, opinions, and data contained in all publications are solely those of the individual author(s) and contributor(s) and not of MDPI and/or the editor(s). MDPI and/or the editor(s) disclaim responsibility for any injury to people or property resulting from any ideas, methods, instructions, or products referred to in the content.

Article

High-Resolution DLP 3D Printing for Complex Curved and Thin-Walled Structures at Practical Scale: Archimedes Microscrew

Chih-Lang Lin [1,2], Jun-Ting Liu [3] and Chow-Shing Shin [3,*]

[1] Center for General Education, Central Taiwan University of Science and Technology, Taichung City, 40601, Taiwan

[2] Department of Automatic Control Engineering, Feng Chia University, Taichung City, 407802, Taiwan

[3] Department of Mechanical Engineering, National Taiwan University, Taipei City, 106319, Taiwan

* Correspondence: csshin@ntu.edu.tw; Tel.: +886-2-33662724

Abstract

As 3D printing becomes increasingly prevalent in microfluidic system fabrication, the demand for high precision has become critical. Among various 3D printing technologies, light-curing-based methods offer superior resolution and are particularly well-suited for fabricating microfluidic channels and associated micron-scale components. Two-photon polymerization (TPP), one such method, can achieve ultra-high resolution at the submicron level. However, its severely limited printable volume and high operational costs significantly constrain its practicality for real-world applications. In contrast, digital light processing (DLP) 3D printing provides a more balanced alternative, offering operational convenience, lower cost, and print dimensions that are more compatible with practical microfluidic needs. Despite these advantages, most commercial DLP systems still struggle to fabricate intricate, high-resolution structures—particularly curve, thin-walled, or hollow ones—due to over-curing and interlayer adhesion issues. In this study, we developed a projection micro-stereolithography (PμSL) system based on DLP technology and fine-tuned its parameters to overcome limitations in printing precise and intricate structures. For demonstration, we selected an Archimedes microscrew as the target structure, as it serves as a key component in microfluidic micromixers. Based on our previous study, the most effective design was selected and fabricated in accordance with practical microfluidic dimensions. The PμSL system developed in this study, along with optimized parameters, provides a reference for applying DLP 3D printing in high-precision microfabrication and advancing microfluidic component development.

Keywords: projection micro-stereolithography (PμSL); DLP 3D printing; microfluidic component; Archimedes microscrew; photo-polymerization

1. Introduction

Three-dimensional (3D) printing, or additive manufacturing (AM), has rapidly expanded beyond prototyping and now plays a vital role in biomedical, electronic, and materials science applications [1–6]. Among these applications, the use of 3D printing for fabricating microfluidic chips has attracted growing interest [7,8], where the demand for higher printing resolution and precision has become paramount. In particular, recent developments in three-dimensional micromixers [9–14] have provided promising solutions for efficient mixing in microchemical processing, microfluidic analysis, and micro total analysis systems (μ-TAS). In various 3D printing techniques, light-curing-based methods offer superior resolution [15], making them particularly suitable for fabricating precise microfluidic systems and related components. Their complex 3D architectures, which are difficult to fabricate using conventional methods, can instead be realized through 3D printing technologies.

© 2025 by the author(s). Distributed under a Creative Commons CC BY license.

Preprints.org (www.preprints.org) | NOT PEER-REVIEWED | Posted: 24 June 2025 doi:10.20944/preprints202506.1976.v1

In our previous works [16,17], we designed an Archimedean micromixer and demonstrated rapid mixing over a short channel length can be achieved. It was fabricated using two-photon polymerization (TPP) 3D printing. Although TPP successfully fabricated highly intricate and mechanically robust 3D micromixers, its limited printable volume and high operational costs severely constrain its practicality for broader micro-fluidic applications. For instance, microfluidic channels often range from tens to hundreds of micrometers in width and extend approximately 1–2 cm in length [18–21]. Under such conditions, using TPP with a typical resolution of 0.1–0.3 μm [22,23] to fabricate even a small 1 mm^3 structure can take a prohibitively long time. This limitation in scalability makes it difficult for TPP to be adopted widely in practical settings.

To address these limitations, Digital Light Processing (DLP) 3D printing has gradually become a promising mainstream approach for microfluidic device fabrication, owing to its advantages such as lower cost, greater accessibility, and printable volumes more suitable for practical applications [24–26]. However, DLP systems still face considerable challenges when printing complex geometries, especially curve, thin-walled, or hollow structures. These difficulties often lead to printing failures due to over-curing [27] and insufficient inter-layer adhesion [28], which in turn results in dimensional inaccuracies, gluing together of features in close proximity, or weak bonding between layers. Such issues become even more pronounced when fabricating structures like Archimedean micromixers, which feature spiral manifolds and closely spaced thin-walled elements that must remain clearly separated to maintain unobstructed internal flow paths [17]. Overcoming these challenges requires meticulous tuning of printing parameters to ensure structural fidelity and functional performance.

In this study, we customized a DLP 3D printer to develop a projection micro-stereolithography (PμSL) system and finely tuned its printing parameters to address the challenges of fabricating high-resolution and intricate microstructures. A three-dimensional Archimedes microscrew, previously proposed and validated in our earlier work at the micrometer scale using TPP [17], was redesigned to conform to commonly used microfluidic system scales. Preliminary test printing will be carried out first to evaluate the limitations on wall separation, wall thickness, and height. Eventually, the microscrew geometry was finalized based on the design guidelines established in our previous study and subsequently realized using the PμSL system.

2. Materials and Methods

2.1. Photo-Curable Resin

The resin used is a mixture of Photomer 4012, Photomer 4017, Photomer 4028, and Photomer 8127. Preliminary tests on different compositions suggested that a weight ratio of 8:1:1:1 yields optimal performance. Omnirad 819 (2 wt%) was added as the photoinitiator. All resin components and the photoinitiator were supplied by IGM Resins (IGM Resins International Trading Taiwan Ltd., Taoyuan, R.O.C.). Additionally, Sudan I (0.15 wt%, Sigma-Aldrich, Neihu, Taipei, R.O.C.) was added as a UV absorbent to limit the curing depth.

2.2. PμSL Printing System

A modified commercial digital light processing projector (P1500, ACER, Taipei, ROC) is modified to generate patterned images for 3D printing via photo-polymerization. The digital micromirror device (DMD) of the projector consists of 1920 × 1080 pixels. The major modification involved inverting and repositioning the projector lens assembly to reduce the projected image size to 4.3 mm × 2.42 mm, which also falls within the commonly used dimensions of microfluidic systems. The resulting pixel resolution is 2.2 μm × 2.2 μm. This modified projection-based 3D printing system can be classified as a Projection micro-Stereolithography (PμSL) system, in which structures are fabricated through layer-by-layer curing of a photocurable resin by the ultraviolet component of the dynamically projected images.

The top surface of the print platform is initially aligned with the resin surface. During printing, the platform is lowered into the resin bath in discrete steps. Following each descending step, the

© 2025 by the author(s). Distributed under a Creative Commons CC BY license.

Preprints.org (www.preprints.org) | NOT PEER-REVIEWED | Posted: 24 June 2025 doi:10.20944/preprints202506.1976.v1

appropriate image is projected. This enables layer-by-layer buildup of the object. A top-down configuration (Figure 1) is employed, which eliminates the need for peeling from a release film. This not only saves the overall print time but also prevents damage to previously cured delicate structures during detachment from the release film, thereby enabling more precise and higher-resolution printing. As a result, the system is particularly suitable for fabricating delicate microscale features. Calibration of the print platform motion indicates that a descending step size of 0.6 μm can be achieved with high reproducibility and accuracy.

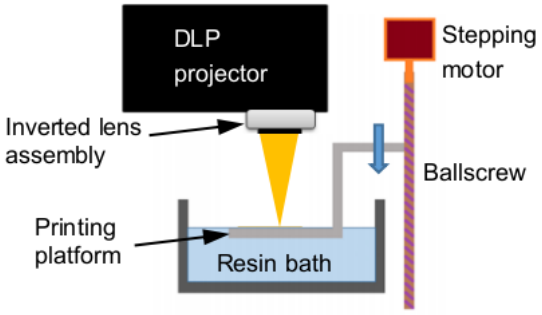

Figure 1. Schematic diagram of the PμSL 3D printing system setup.

2.3. Method for Evaluating Printable Features

To evaluate the printing accuracy and limitations of the current system, thin walls with various thicknesses and heights were test-printed. Two test-print designs were employed, as shown in Figure 2. In Figure 2(a), six vertical walls are connected by two horizontal ties that pass through each wall, providing structural support to help them stand upright in a stable manner. The horizontal separation d and height h of the walls were kept constant at 400 μm and 350 μm, respectively, while the wall thickness t varied from 10 μm to 50 μm across different prints. In Figure 2(b), four pairs of vertical walls are shown with a constant thickness of 10 μm. The horizontal separations between successive pairs of walls are 180, 200, 250, and 300 μm, respectively. A series of wall heights h, ranging from 100 to 500 μm, were tested in different prints.

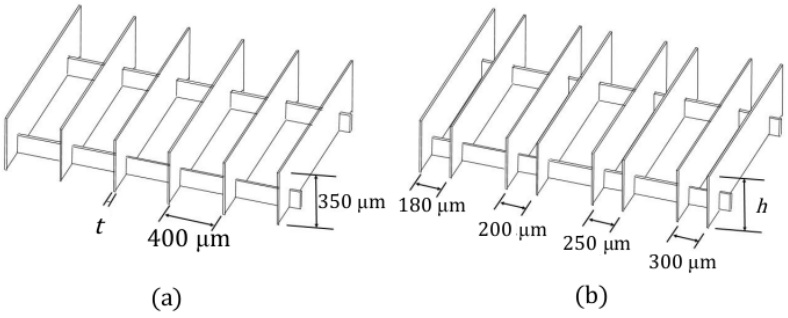

Figure 2. Test print designs for testing (a) wall thickness t (= 10 μm to 50 μm) and (b) wall height h (= 100 μm to 500 μm).

2.4. Design and Printing Strategy of Archimedes Microscrew

A three-dimensional solid model of the Archimedes microscrew is generated by simultaneously rotating and translating a rectangular cross-section along the dotted path shown in Figure 3(a), resulting in a geometry that forms the screw surface. Figure 3(b) illustrates the outcome of one complete turn. Based on this design pattern, different screw turns can be constructed. A rectangular cuboid with a height (H) to width (W) ratio of 0.75 is extracted from the circular-sectioned screw, as shown in Figure 3(c). The resulting microscrew cuboid (Figure 3(d)) is then placed into the rectangular cross-sectional flow manifolds formed by two side walls.

© 2025 by the author(s). Distributed under a Creative Commons CC BY license.

Preprints.org (www.preprints.org) | NOT PEER-REVIEWED | Posted: 24 June 2025 doi:10.20944/preprints202506.1976.v1

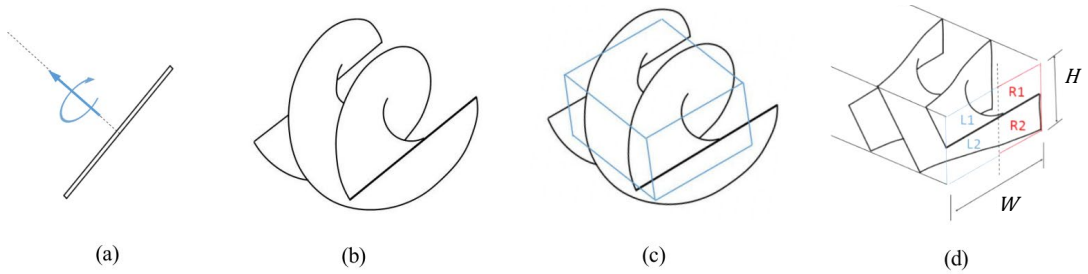

Figure 3. Generation of the Archimedes microscrew model for printing: (a) rectangular generator undergoing simultaneous rotation and translation; (b) resulting screw surface after one full turn; (c) rectangular cuboid section extracted for use; (d) final microscrew with rectangular cross-sectional throughput.

The solid model is then horizontally sliced into multiple layers, and the image of each layer is recorded. The total number of layers corresponds to the overall height of the model divided by the thickness of each printing layer. Figure 4 shows examples of the sliced images at three different heights of the model. These successive sliced images are projected onto the printing stage, which is progressively lowered into the resin in discrete steps.

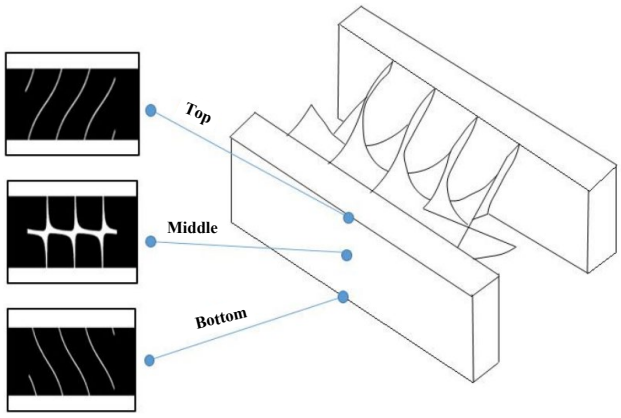

Figure 4. Example of some of the slices of the solid model at three different depths.

3. Results and Discussions

3.1. Wall Thickness and Structural Stability

Figure 5 shows scanning electron micrographs (SEM) of printed structures based on the design in Figure 2(a), with wall thicknesses of 10 μm and 20 μm, respectively. In the 10 μm case (Figure 5(a)), the low stiffness of the thin walls makes them prone to localized buckling, resulting in visible bulging deformation. This phenomenon can be attributed to volumetric contraction associated with polymerization, combined with the layer-by-layer curing process of the current 3D printing technique, which may induce non-uniform residual stress. As the wall thickness increases, its rigidity improves, allowing it to resist buckling more effectively. Consequently, the structure appears nearly normal, and the printed walls become well-defined and structurally sound, as shown in Figure 5(b).

© 2025 by the author(s). Distributed under a Creative Commons CC BY license.

Preprints.org (www.preprints.org) | NOT PEER-REVIEWED | Posted: 24 June 2025 doi:10.20944/preprints202506.1976.v1

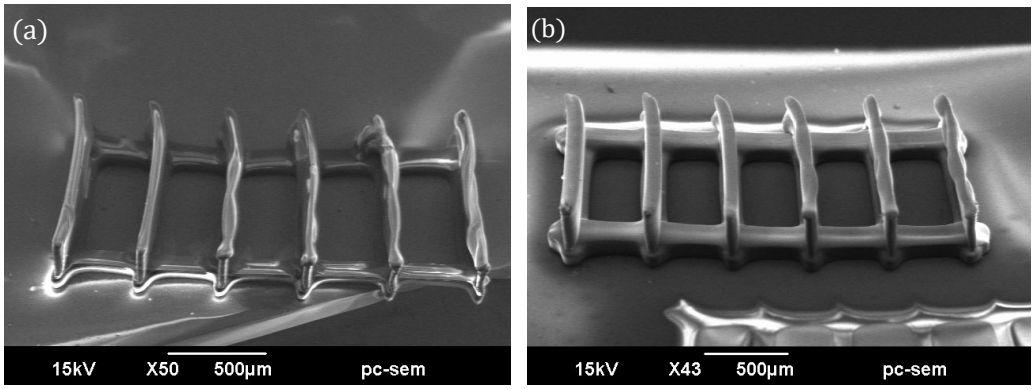

Figure 5. Printed results of the design shown in Fig. 2(a) with designed wall thicknesses of (a) 10 μm and (b) 20 μm.

Beyond deformation, dimensional inaccuracy is also evident. Measurements show that the printed walls are consistently thicker than their corresponding design values. Figure 6 compares the design thicknesses with the actual printed results, revealing that the final wall thicknesses are generally three to four times greater than intended. This discrepancy may arise from three primary factors.

First, the light emitted from each pixel on the Digital Micromirror Device (DMD) does not exhibit a sharply bounded unit function distribution but rather follows a Gaussian profile [29,30]. The light intensity gradually decays and remains non-zero even at a considerable distance beyond the pixel edge. When neighboring pixels are activated simultaneously, such as across a wall's width, the overlap of beyond-the-pixel light may raise the total intensity sufficiently to initiate unintended polymerization outside the designed boundary.

Second, the resin system used in this work, like most materials employed in stereolithographic 3D printing, cures via a free radical polymerization mechanism [31]. These free radicals can diffuse a short distance from their origins before reacting, contributing to a spatially extended polymerization zone [32].

Third, excessive polymerization may also result from overlapping exposures during the layer-by-layer process. In the current setup, light converges at the focal plane where curing is intended. Below this plane, the beam diverges and becomes weaker due to the inherent divergence and resin absorption. Although the intensity in these regions is insufficient for polymerization during a single exposure, repeated exposures allow free radicals to accumulate. Over time for a number of successive exposures, the radical concentration may exceed the polymerization threshold even in unintended areas, leading to further broadening of the cured walls.

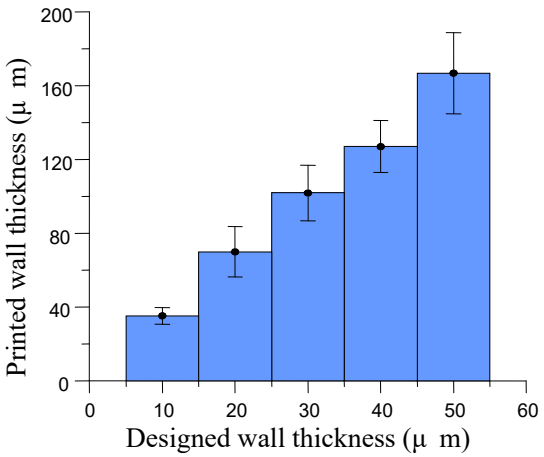

© 2025 by the author(s). Distributed under a Creative Commons CC BY license.

Preprints.org (www.preprints.org) | NOT PEER-REVIEWED | Posted: 24 June 2025 doi:10.20944/preprints202506.1976.v1

Figure 6. Printed results of the design shown in Figure 2(a) with designed wall thicknesses of (a) 10 μm and (b) 20 μm.

3.2. Effect of Wall Height and Gap Spacing on Printable Resolution

Figure 7 shows the printed results based on the design in Figure 2(b), with wall heights (h) ranging from 100 to 500 μm and a fixed wall thickness of 10 μm. In each print, the designed horizontal separations between adjacent wall pairs, from left to right, are 180 μm, 200 μm, 250 μm, and 300 μm, respectively. The actual gap widths are smaller than the designed values due to the wall broadening discussed earlier. At a wall height of 100 μm (Figure 7(a)), the gaps between each wall pair are generally visible, except near the intersections between the horizontal reinforcing ties and the walls. The excessive curing observed there around the corners can be attributed to previously mentioned factors: the superposition of beyond-the-pixel light, short-range diffusion of free radicals, and accumulation of free radicals from successive exposures. Narrow gaps can confine free radicals, facilitating their accumulation. When the wall height increases to 200 μm (Figure 7(b)), the spaces in the leftmost 180 μm gap and part of the 200 μm gaps are no longer fully open. Interestingly, the localized bulging observed in Figure 5(a) does not appear here, likely due to the higher stiffness of shorter walls. Vertical wall profiles remain clearly defined, suggesting that the filling occurs only up to a portion of the wall height. The excess material deep within the gaps may be a residual resin that cannot be completely removed due to surface tension in these narrow intervals. As the wall height increases to 300 μm (Figure 7(c)) and beyond (Figure 7(d) and (e)), the aforementioned issues persist. At a wall height of 500 μm, the entire 200 μm gap becomes filled. Moreover, from a height of 300 μm onward, localized wall bulging begins to appear, indicating that wall stiffness is no longer sufficient to withstand buckling caused by the residual curing stress.

The above printing results suggest that to ensure a through flow, the pitch of the Archimedes microscrew must be large enough. Considering the screw profile is much more complicated than a vertical wall, a pitch of 280 μm is chosen to generate the microscrew for a 500 μm channel width. For a 800 μm channel width, the pitch is increased in proportion to 480 μm.

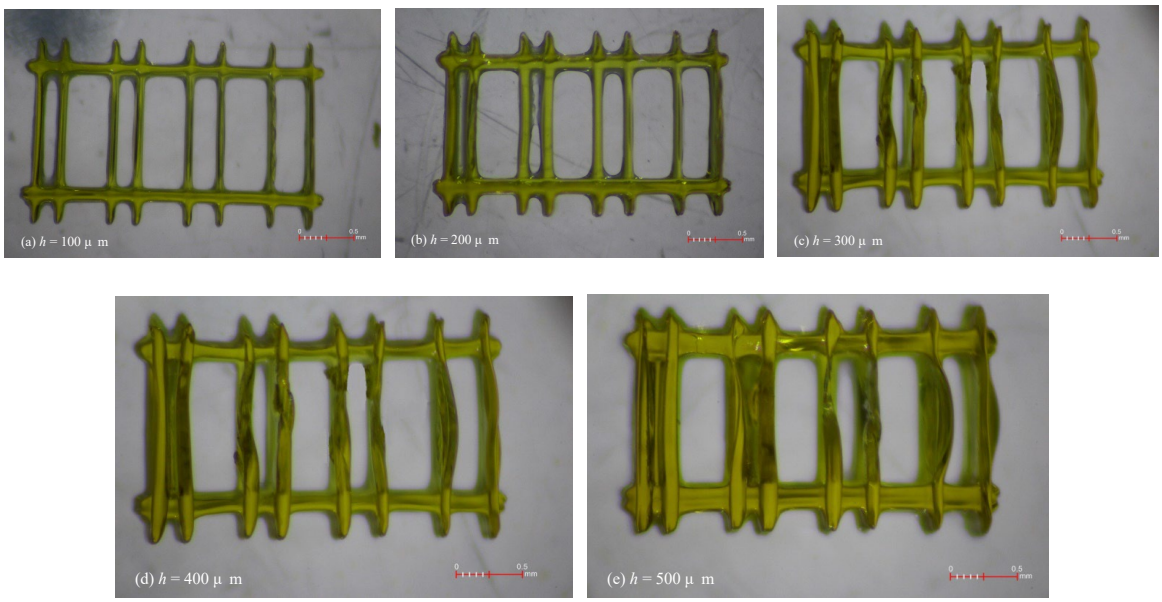

Figure 7. Print results of the design in Figure 2 (b) with designed wall thickness of 10 μm and height of (a) 100 μm; (b) 200 μm; (c) 300 μm; (d) 400 μm; (e) 500 μm.

3.3. Realization of the Archimedes Micoscrew

According to previous findings, the geometric parameters of a 2-turn Archimedes microscrew were carefully selected to ensure structural integrity and to prevent over-polymerization in critical

© 2025 by the author(s). Distributed under a Creative Commons CC BY license.

Preprints.org (www.preprints.org) | NOT PEER-REVIEWED | Posted: 24 June 2025 doi:10.20944/preprints202506.1976.v1

regions. Specifically, wall thicknesses of at least 20 μm were used to avoid deformation caused by residual stress, as previously demonstrated. Furthermore, to prevent unintended closure of flow gaps resulting from optical broadening and radical diffusion, the screw pitch was optimized to ensure sufficient spacing between adjacent wall segments in accordance with earlier guidelines. To ensure clear separation between neighboring screw threads and sufficient structural stiffness, a pitch of 280 μm and 480 μm was adopted for the 500 μm- and 800 μm-wide flow channel widths, respectively. The designed microscrew profiles were then fabricated using the same PμSL printing system described earlier.

Figure 8 presents SEM images of the printed Archimedes microscrew structures with side walls. The screw elements were well-resolved, with no significant distortion or merging between adjacent threads, indicating that the chosen geometric parameters successfully mitigated the effects of optical overexposure and radical accumulation. Furthermore, structural fidelity and continuity of the microscrew manifold were achieved, which are expected to facilitate sufficient flow and provide a foundation for future mixing applications. It is also noteworthy that the surfaces of the screw threads exhibit wave-like striations along the axial direction. These patterns are characteristic of layer-by-layer additive manufacturing and are generally unavoidable. However, such surface irregularities may be beneficial in the context of microfluidic mixing, as they can introduce additional perturbations to the flow, thereby enhancing mixing efficiency.

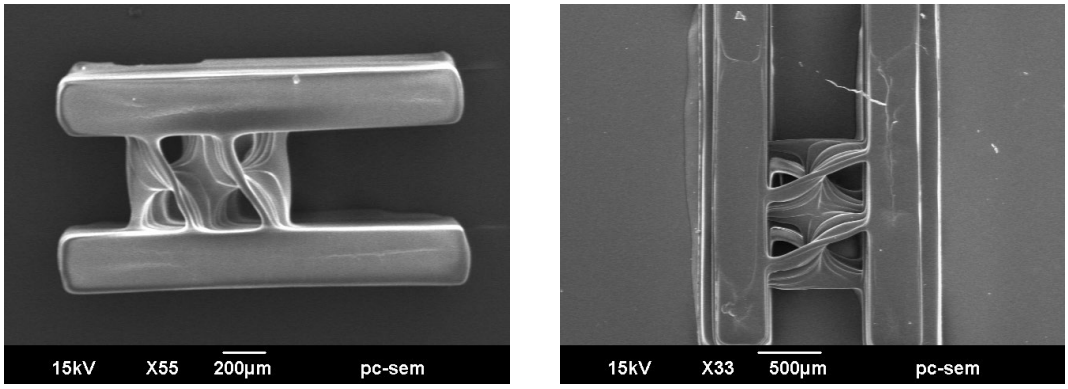

(**a**) (**b**)

Figure 8. SEM images of the printed Archimedean micromixer structures: (a) 500 μm width; (b) 800 μm width.

The printing results of the Archimedes microscrew validate the effectiveness of the design strategy guided by resolution and stability analyses. The investigation of printing parameters demonstrates the feasibility of fabricating complex 3D flow structures using our PμSL system, providing a foundation for the further development of high-performance microfluidic mixing devices.

4. Conclusions

This study investigated the limitations and capabilities of a DLP-based PμSL 3D printing system for fabricating three-dimensional microstructures, with a focus on the realization of complex curved and helical thin-walled structures–specifically, Archimedes microscrew. Through systematic evaluations of printed wall thickness, height, and gap resolution, we identified key parameters that govern structural fidelity and dimensional accuracy. The printable gap between walls becomes narrower than designed, especially as the wall height increases. This deviation is attributed to a combination of optical spreading beyond pixel boundaries, free radical diffusion, and cumulative polymerization effects from layer-to-layer exposures. Based on these insights, Archimedes microscrews were successfully both designed and printed using optimized geometric parameters. The fabricated structures demonstrate clear separation between adjacent screw threads without structural fusion or collapse, confirming the feasibility of using this printing strategy for complex 3D microfluidic devices. The findings in this study not only offer practical guidelines for printing

© 2025 by the author(s). Distributed under a Creative Commons CC BY license.

Preprints.org (www.preprints.org) | NOT PEER-REVIEWED | Posted: 24 June 2025 doi:10.20944/preprints202506.1976.v1

resolution-sensitive microstructures but also highlight the potential of DLP-based 3D printing in advancing the design and fabrication of integrated microfluidic components.

Author Contributions: "Conceptualization, C.-S.S. and C.-L.L.; methodology, C.-S.S. and C.-L.L.; software, C.-S.S. and J.-T.L.; validation, C.-S.S. and J.-T.L.; formal analysis, J.-T.L.; investigation, J.-T.L.; resources, C.-S.S.; data curation, C.-S.S., J.-T.L. and C.-L.L.; writing—original draft preparation, C.-S.S. and C.-L.L.; writing—review and editing, C.-S.S. and C.-L.L.; visualization, J.-T.L.; supervision, C.-S.S. and C.-L.L.; project administration, C.-S.S.; funding acquisition, C.-S.S. All authors have read and agreed to the published version of the manuscript.".

Funding: This research was funded by the Ministry of Science and Technology, ROC, through the projects MOST 107-2221-E-002 -114 -MY3 and NSTC 112-2221-E-002 -227 -MY2.

Data Availability Statement: The data involved in this study have basically been presented in this paper. Further details and queries may be directed at the corresponding author.

Acknowledgments: he authors would like to thank the Ministry of Science and Technology, ROC, for funding.

Conflicts of Interest: The authors declare no conflicts of interest.

Abbreviations

The following abbreviations are used in this manuscript:

AM	Additive Manufacturing
DLP	Digital Light Processing
PμSL	Projection micro-stereolithography
TPP	Two-Photon Polymerization

References

1. Hosseinabadi, H. G.; Nieto, D.; Yousefinejad, A.; Fattel, H.; Ionov, L.; Miri, A. K. Ink material selection and optical design considerations in DLP 3D printing. *Applied Materials Today* 2023 30, 101721.
2. Derby, B. Printing and Prototyping of Tissues and Scaffolds. *Science* 2012 338, 921–926.
3. Zhang, P.; Lei, I. M.; Chen, G.; Lin, J.; Chen, X.; Zhang, J.; Cai, C.; Liang, X.; Liu, J. Integrated 3D printing of flexible electroluminescent devices and soft robots. *Nature Communications* 2022 13, 4775.
4. Vaezi, M.; Seitz, H.; Yang, S. A review on 3D micro-additive manufacturing technologies. *The International Journal of Advanced Manufacturing Technology* 2013 67, 1721–1754.
5. Ge, Q.; Jian, B.; Li, H. Shaping soft materials via digital light processing-based 3D printing: A review. *Forces in Mechanics* 2022 6, 100074.
6. Lewis, J. A.; B. Y. Ahn, "Three-dimensional printed electronics. *Nature* 2015 518, 42–43.
7. Kabandana, G. K. M.; Zhanga, T.; Chen, C. Emerging 3D printing technologies and methodologies for microfluidic development. *Analytical Methods* 2022 14, 2855–2906.
8. Lewis, J. A.; Ahn, B. Y. Comparing Microfluidic performance of three-dimensional (3D) printing platforms. *Analytical Chemistry* 2017 89, 3858–3866.
9. Lim, T. W.; Son, Y.; Jeong, Y.J.; Yang, D.-Y., Kong, H.-J.; Lee, K. S.; Kimd, D.-P. Three-dimensionally crossing manifold micro-mixer for fast mixing in a short channel length. *Lab Chip* 2011 1, 100–103.
10. Liu, Y.-J.; Chen, P.-Y.; Yang, J.-Y.; Tsou, C.; Lee, Y.-H.; Baldeck, P. L.; Lin, C.-L. Three-dimensional passive micromixer fabricated by two-photon polymerization for microfluidic mixing. *Sensors and Materials* 2014 26, 39–44.
11. Lin, Y.; Gao, C.; Gritsenko, D.; Zhou, R.; Xu, J.; Soft lithography based on photolithography and two-photon polymerization. *Microfluidics and Nanofluidics* 2018 22, 97.
12. Liu, B.; Ran, B.; Chen, C.; Shi, L.; Liu, Y.; Chen H.; Zhu, Y. A low-cost and high-performance 3D micromixer over a wide working range and its application for high-sensitivity biomarker detection. *Reaction Chemistry & Engineering* 2022 7, 2334–2347.

© 2025 by the author(s). Distributed under a Creative Commons CC BY license.

Preprints.org (www.preprints.org) | NOT PEER-REVIEWED | Posted: 24 June 2025 doi:10.20944/preprints202506.1976.v1

13. Z. Wang, X. Yan, Q. Zhou, Q. Wang, D. Zhao, H. Wu, "A directly moldable, highly compact, and easy-for-integration 3D micromixer with extraordinary mixing performance," Analytical Chemistry 2023 95 (23), 8850–8858.
14. Alzoubi, M. A.; Al-Ketan, O.; Muthusamy, J.; Sasmito, A. P.; Poncet, S. Mixing performance of T-shape micromixers equipped with 3D printed Gyroid matrices: A numerical evaluation. *Results in Engineering* 2023 17, 100811.
15. Quan, H.; Zhang, T.; Xu, H.; Luo, S.; Nie, J.; Zhu, X. Photo-curing 3D printing technique and its challenges. *Bioactive Materials* 2020 5, 110–115.
16. Lin, C.-L.; Liu, Y.-J.; Lin, Z.-D.; Wu, B.-L.; Lee, Y.-H.; Shin, C.-S.; Baldeck, P.-L. Laser direct writing 3D structures for microfluidic channels: flow meter and mixer. Proc. SPIE 9320, Microfluidics, BioMEMS, and Medical Microsystems XIII 5, San Francisco, California, United States, March 2015, 93200H.
17. Shin, C.-S.; Baldeck, P. L.; Nie, Y.-M.; Lee, Y.-H.; Lin, Z.-D.; Chiang, C.-C.; Lin, C.-L. Design and evaluation of a 3D multi-manifold micromixer realized by a double-Archimedes-screw for rapid mixing within a short distance. *Journal of the Taiwan Institute of Chemical Engineers* 2021 120, 59–66.
18. Wei, Y. C.; Chen, F.; Zhang, T.; Chen, D. Y.; Jia, X.; Wang, J. B.; Guo, W.; Chen, J. Vascular smooth muscle cell culture in microfluidic devices. *Biomicrofluidics* 2014 8, 046504.
19. Green, J. V.; Kniazeva, T.; Abedi, M.; Sokhey, D. S.; Taslim, M. E.; Murthy, S. K. Effect of channel geometry on cell adhesion in microfluidic devices. *Lab on a Chip* 2009 9, 677–85.
20. Sun, Y.-S. Comparison of Chip Inlet Geometry in Microfluidic Devices for Cell Studies. *Molecules* 2016 21, 778.
21. Pisapia, F.; Balachandran, W.; Rasekh, M. Organ-on-a-Chip: Design and Simulation of Various Microfluidic Channel Geometries for the Influence of Fluid Dynamic Parameters. *Applied Sciences* 2022 12, 3829.
22. Zhou, X.; Hou, Y.; Lin, J. A review on the processing accuracy of two-photon polymerization. *AIP Advances* 2015 5, 030701.
23. O'Halloran, S.; Pandit, A.; Heise, A.; Kellett, A. Two-Photon Polymerization: Fundamentals, Materials, and Chemical Modification Strategies. *Advanced Science* 2023 10, 202204072.
24. Hosseinabadi, H. G.; Nieto, D.; Yousefinejad, A.; Fattel, H.; Ionov, L.; Miri, A. K. Ink material selection and optical design considerations in DLP 3D printing. *Science* 2012 338, 921–926.
25. Than, A.; Liu, C.; Chang, H.; Duong, P. K.; Cheung, C. M. G.; Xu, C.; Wang X.; Chen, P. Self-implantable double-layered micro-drugreservoirs for efficient and controlled ocular drug delivery. *Nature Communications* 2018 9, 4433.
26. Yi, R.; Wu, C.; Liu, Y.-J.; He, Y.; Wang, C. C. L. Delta DLP 3D printing of large models. *IEEE Transaction on Automation Science and Engineering* 2018 15, 1193–1204.
27. Böcherer, D.; Li, Y.; Rein, C.; Corredor, S. F.; Hou, P.; Helmer, D. High-resolution 3D printing of dual-curing thiol-ene/epoxy system for fabrication of microfluidic devices for bioassays. *Advanced Functional Mateialsr* 2024 34, 2401516.
28. Zhu, G.; Hou, Y.; Xu, J.; Zhao, N. Digital Light Processing 3D Printing of Enhanced Polymers via Interlayer Welding. *Macromollecular Rapid Communications* 2022 43, e2200053.
29. Lachetta, M.; Sandmeyer, H.; Sandmeyer, A.; Esch, J. S. a.; Huser, T.; Müller, M. Simulating digital micromirror devices for patterning coherent excitation light in structured illumination microscopy. *Philosophical Transactions A* 2021 379, 20200147.
30. Weng, C.-L.; Wu, C.-Y.; Lee, Y.-C. Enhanced corner sharpness in DMD-based scanning maskless lithography using optical proximity correction and genetic algorithm. *Optics Express* 2024 32, 45357–45372.
31. Mukhtarkhanov, M.; Perveen, A.; Talamona, D. Application of Stereolithography Based 3D Printing Technology in Investment Casting. *Micromachines* 2020, 11, 946.
32. Yu, C.; Schimelman, J.; Wang, P.; Miller, K. L.; Ma, X.; You, S.; Guan, J.; Sun, B.; Zhu, W.; Chen, S. Photopolymerizable Biomaterials and Light-Based 3D Printing Strategies for Biomedical Applications. *Chemical Reviews* 2020 120, 10695-10743.

Disclaimer/Publisher's Note: The statements, opinions and data contained in all publications are solely those of the individual author(s) and contributor(s) and not of MDPI and/or the editor(s). MDPI and/or the editor(s)

© 2025 by the author(s). Distributed under a Creative Commons CC BY license.

Preprints.org (www.preprints.org) | NOT PEER-REVIEWED | Posted: 24 June 2025 doi:10.20944/preprints202506.1976.v1

disclaim responsibility for any injury to people or property resulting from any ideas, methods, instructions or products referred to in the content.

© 2025 by the author(s). Distributed under a Creative Commons CC BY license.